Toward lean minimally invasive robotic surgery

Matteo Zoppi, Mohammed Aamir Khan, Felix Schäfer
and Rezia Molfino*

University of Genoa, Deptartment of Mechanics and Machine Design, PMAR Robot Design Research Group, Genoa, Italy

SUMMARY

Developed minimally invasive surgical (MIS) robots are large multi-arm, multipurpose systems requiring significant investments that limit their availability in hospitals. A larger distribution of MIS robots with benefit for patients might be achieved improving their modularity and scalability so that smaller hospitals or medical centers could decide for a simpler and lower cost setup for a limited number of treatments only, while centers with higher funding could have more systems dedicated to different classes of operations. In line with this statement the paper proposes the paradigm of lean MIS system comprising a scalable set of modular, agile, small size single-instrument robots with limited life cycle cost. Miniaturization of instruments can further reduce invasiveness of procedures and one promising research direction is needle laparoscopic surgery, which can be applied to classes of operations on small regions requiring small force interaction with the patient. In the paper the development of a lean single-instrument manipulator for needlescopic surgery is presented and a new master concept for accurate restitution of surgical force proposed and discussed.

KEYWORDS: Surgical robotics; Minimally invasive surgery; Needlescopic surgery.

1. Introduction

Surgical practice evolves in parallel with the advancements in the technical domains providing enabling technologies and tools.

Robotics enabled the passage from manual laparoscopic surgery to minimally invasive robotic surgery (MIRS).[1–3] In laparoscopic surgery tissues are manipulated using instruments inserted along trocars through small incisions (keyholes). Each instrument slides along the trocar (1 translation) and rotates about the keyhole (3 rotations). Various additional degrees of freedom (DOF) may be available at the tip (wrist) or along the instrument to orient the surgical tool. In MIRS instead of directly handling the instruments the surgeon uses haptic interfaces to operate robotic manipulators maneuvering the instruments. The control system receives commands from the haptic interfaces, controls the surgical manipulators, collects and processes data, and provides to the surgeon information related to the operation.[4,5] Improved and reliable information is made available to the surgeon based on a multi-sensorial system comprising visual and force feedback fused to other information traditionally unavailable on the theater, e.g., from magnetic resonance imaging (MRI).

MIS has become standard for various surgical and diagnostic procedures for the clear benefit to patients who suffer minimum trauma to healthy tissues resulting in less postoperative pain and shorter hospitalization. Robotic systems overcome the main limitations of manual laparoscopy. Instruments can have more degrees of freedom yielding higher dexterity. Intelligent control can filter surgeon hand tremor and increase accuracy by motion scaling. Three-dimensional imaging and an appropriate master architecture may improve surgeon hand–eye coordination making the operation more intuitive.

Several robotic systems for laparoscopic surgery have been proposed or are already commercially available. The most popular commercial system is the da Vinci comprising a surgeon console, a patient-side cart and EndoWrist instruments.[6] Sitting at the console the surgeon sees the surgical environment in 3D vision and guides the robot arms on the cart by means of two joysticks and foot-pedals. The slave robot on the cart usually has three arms, two for instruments and one for endoscope; an optional fourth arm may be also used. Each arm has a standard interface for EndoWrist instruments. EndoWrist instruments comprise a tendon driven 2-DOF wrist to orient the tool. Instruments' diameters range between 5–8 mm and the incision between 10–20 mm.

Another commercial system no more available was ZEUS with the main difference that instruments did not have wrist freedoms.

Besides these systems a lot of research effort is dedicated to laparoscopic surgery.[7]

The Raven surgical robot from the University of Washington[8] uses a 3R spherical mechanism and provides two rotations about the keyhole and trocar translation. The system supports EndoWrist instruments with embedded wrist. The slave robot is 6-DOF cable actuated with all actuators in the base. Military application is foreseen and main design requirements are size and transportability. Phantom haptic interfaces are used as masters and tele-surgery is supported.[9]

The UC Berkeley/UCSF Telesurgical Workstation[10] comprises a 6-DOF robotic manipulator for laparoscopic surgery with 2-DOF wrist. The instrument has a diameter of 10 mm. The yaw motion is actuated by tendons whereas

* Corresponding author. E-mail: molfino@dimec.unige.it

roll and grasping motion are hydraulically actuated. As master a modified Impulse Engine 3000 (Immersion) is used providing force feedback on 4-DOF.

Another master-slave system is proposed in ref. [11]. The master provides 6-DOF plus grasping and a parallel link mechanism keeps handle orientation fixed. Servo motors transmit force feedback information to the surgeon. The slave robotic system consists of three arms, two for the instruments, one for the camera. For safety reasons the insert position at the keyhole is mechanically guaranteed.

The DLR in Germany develops the *Miro* robot which is the second generation of *KineMedic*.[12] *Miro* is a redundant lightweight arm with high payload-to-weight ratio and a wide range of applications from accurate operations like setting holes for bone screws to multi-robot MIS. The *KineMedic* concept is also further developed in the ongoing project AccuRobAs (Accurate Robot Assistant – IST-2005-2.6.1) focusing on improvement of accuracy and surgical performance figures. Depending on the application, the modular architecture allows to use one arm for open surgery or up to three arms together for MIS.

In ref. [13] the Massachusetts Institute of Technology presents The Black Falcon, an 8-DOF slave manipulator guided by a modified 7-DOF Phantom master with force feedback on 3-DOFs. A double 4-bar linkage constraints the instrument to rotate about the incision point without lateral displacements.

MIS invasiveness can be further reduced for some classes of operations requiring interaction forces with tissues smaller than the ones currently provided by the smallest standard (5 mm diameter) laparoscopic tools. Smaller tools called needlescopes (2–3 mm diameter) are used reducing the size of incisions on the patient's body and the internal space required to carry out the operations.

Due to the small diameter the applicable forces are lower than those for laparoscopic instruments and elasticity has to be considered for safety issues. These disadvantages caused the opinion that needlescopic surgery is only applicable for diagnostics, but it turned out that also therapeutic procedures can be performed. As described in ref. [14] several operations have been performed with 3 mm needlescopic instruments, e.g., cholecystectomy, Nissen fundoplication, Heller myotomy, and splenectomy. Compared to the same operations performed with laparoscopic instruments, postoperative pain, hospital stay and finally also the costs are reduced with no apparent increase in operative time. Surgeons already experienced with laparoscopic surgery could easily adapt to the new instruments, whereas it is suggested for new surgeons not to start with needlescopic instruments.

Note that there is a strict interdependence between procedure and instruments with cross influence: tools serve the procedure and the procedure is defined on the basis of available technology and realizable tools. Firm requirements come from mandatory actions to be carried out for the treatment of the disease, e.g., full ablation of a certain part of an organ. It is generally difficult to clearly identify such firm requirements and parallel evolution of procedures and tools may continuously increase the number of treatments that can be carried out with smaller tools (compared to the smallest current laparoscopic tools) able to exert smaller forces.

In line with this evolution of MIS robotics to needlescopic surgery, the paper presents an intrinsically safe manipulator with parallel architecture and a new design for a 6-DOF force feedback haptic master. The master reflects all the laparoscopic constraints already in the mechanism architecture and gives the surgeon the feeling as if his hand was inside the patient's body.

2. Lean Needlescopic MIS Systems

In spite of extensive research, few robotic MIS systems are fully commercially available and are expensive and bulky.

Areas of application and procedures which can be carried out with robotic MIS increase according to the scientific and technological advancements in the related fields. The complexity of the in use systems is an obstacle and new important requirements become transportability and leanness. The concept of lean MIS system emerges: it involves a higher level of scalability and modularity than in the available MIS systems. Specialization is considered as a potential advantage: instead of multipurpose units able to carry out almost any type of operation lean systems can be used for classes of operations with the potential benefit to have an overall higher number of systems functioning in hospitals and medical centers and a higher rate of surgical interventions carried out with robotic MIS instead of traditional techniques.

An example of emerging application field is military tele-surgery where lean robotic MIS systems are available on the field and surgeons can operate injured army personnel and civilians from remote.

The increase in procedures that can be carried out with needlescopic MIS may promote the development and diffusion of lean systems. The robotic manipulators operating needlescopic tools can be remarkably smaller than the ones for laparoscopic surgery. The number of tools changes accordingly to the type of operation. Functional requirements generally change and system layouts different from the ones currently adopted in robotic laparoscopic MIS become feasible.

A lean scalable needlescopic MIS system comprises: (a) a variable number of manipulation modules with identical interfaces: to the needlescopic instrument, to the ground support, and for signals and power (Fig. 1a); (b) a ground support (generally passive reconfigurable) able to carry a variable number of manipulation modules and to provide to each of them signal and power interfaces (the architecture of the support can be specifically customized); (c) a set of modular surgical instruments; and (d) a modular haptic surgeon-system interface (master) for each manipulation module.

The control architecture of the lean MIS system is modular, distributed between the manipulation modules, each with a dedicated controller, and the master. The master can support different command schemes for different instruments carried by the manipulation module.

A lean system for needlescopic surgery applying these concepts has been designed at the laboratory of Design and
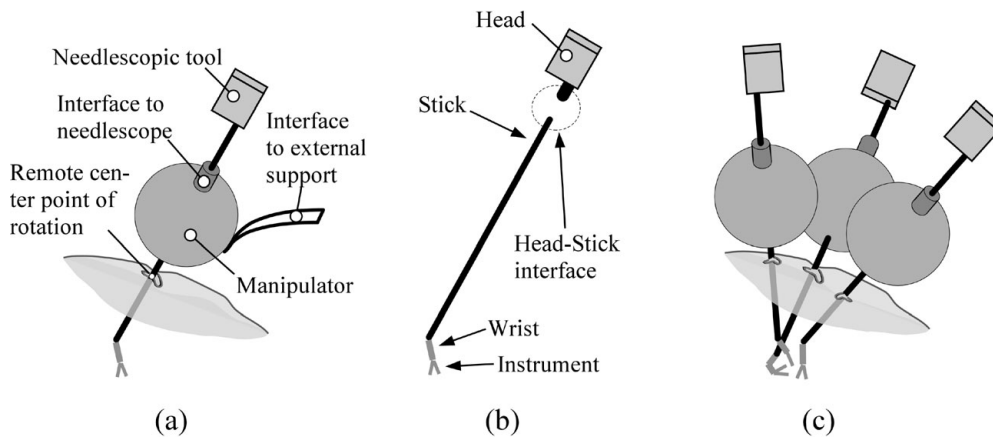
Fig. 1. Schematic of lean robotic needlescopic MIS manipulator (a); detail of modular needlescopic instrument (b); cluster of manipulators operating in the same workspace (c).

Measurements for Automation and Robotics (PMAR), the University of Genoa. The concept of handling the surgical instrument as in open surgery is applied. The haptic interface is designed to replicate the kinematics and constraints of the surgical instrument inserted in the patient's body in order to allow very accurate reflection of forces and feel of the instrument.

The following points out the new concepts about the manipulation modules and the instrument. Design details for the PMAR lean needlescopic system are provided in Section 3 dedicated to the manipulating slave and in Section 4 illustrating the guiding master.

2.1. Manipulation modules
The manipulation module is an actuated mechanism carrying one surgical instrument. The end-effector is a support along which the instrument can be inserted and attached (instrument-support). The motion of the end-effector is of type SP (spherical–prismatic) with the center of spherical motion placed in correspondence of the keyhole: the instrument tilts about the keyhole, rotates about its axis (torsion), and translates parallel to its axis (extrusion). The motion pattern is exactly the one allowed to the instrument and there is no possibility of control errors resulting in translation of the surgical instrument transversally to the keyhole with injure of the patient (as it could happen with a serial 6-DOF or 7-DOF robot controlled to satisfy the keyhole constraint).

More modules are placed near each other on the patient's body so that the instruments they carry can work in the same surgical workspace (Fig. 1c).

Requirements on workspace and placement of the modules are detailed in Section 2.4.

The SP equivalent motion pattern can be generated with three main mechanism layouts:[15] (a) a serial mechanism, e.g., of type (RRR)P (three R-joints with axes crossing at a point and a P-joint) with all joints actuated; (b) a purely parallel or series–parallel[16] SP-equivalent mechanism; (c) a UP-equivalent mechanism (universal-prismatic) to provide tilt and extrusion and a R-equivalent mechanism in series (actuated revolute joint through the center of the U joint) to provide torsion; and (d) a S-equivalent mechanism for tilt and torsion and a P equivalent mechanism (actuated prismatic joint) in series for the extrusion.

A parallel or series-parallel architecture is preferable with respect to the serial architecture and to the architectures with separate actuated joints for torsion or extrusion: only the joints closest to the base are actuated, a remote center point of rotation (CPoR) (the center of the S motion) is normally easy to generate, the instrument is supported by more than one kinematic chain and sufficient accuracy and stiffness can be obtained with relatively small links, the rotational workspace can be large enough.

The rotational workspace does not scale when scaling the mechanism. The geometry of an SP-equivalent parallel or series–parallel mechanism (and then its overall size) is related to the extrusion range and scales proportionally to it.

The overall range of extrusion required comprises two portions: one to insert the instrument inside the patient's body up to the surgical region and one (shorter) used during surgery operations.

In order to keep the size of the mechanism small only the amount of extrusion for surgery should be provided by the parallel SP-equivalent mechanism. The extrusion range for instrument insertion could be provided by an additional actuated prismatic joint in series with the SP mechanism with the drawback to have again an actuated joint on the end-effector of the manipulator. Preferably the instrument is inserted manually at the beginning of the operation and locked to the end-effector of the manipulation module. Manual insertion is preferable also because the surgeon has direct feel of the process, the actuated joint on the end-effector is avoided and the SP-equivalent mechanism can have the smallest possible size.

The design of the manipulation module in Section 3 is developed in accordance.

2.2. Modular needlescopic instruments with MEMS components
Current modular laparoscopic surgical instruments for robotic surgery have head, stick, wrist and tool integrated and not separable and actuation is realized through a mechanical interface from the handling robot. Mechanical solutions

adopted (especially for motion transmission) and fabrication are typical of mesoscale mechanics.

The passage to needlescopic instruments asks for radical changes in mechanics and architecture. An effective architecture is with wrist and tool actuation embedded in the instrument. Each instrument, (Fig. 1b) comprises a head and a stick connected together by an easy-plug interface. The distribution of components between head and stick is suggested also by their duration and sterilization requirements.

The head contains actuators and services for the management of the stick including position sensors required in some cases to control wrist and tool. These components are costly, difficult to sterilize and their life is generally longer than the life of instrument and actuation transmission components. One or few head types distinguished by number of freedoms they actuate can be used for all instruments.

Sticks comprise: (a) the surgical instrument (one specific stick per each type of instrument); (b) a wrist or kinematic chain with with motion suitable for the specific tool carried; (c) mechanical transmissions to transfer actuation from the head to the joints and the tool; and (d) power transmission for the tool, if needed.

Due to the small diameter, meso-scale fabrication techniques cannot be suitably used and parts should be designed for fabrication with MEMS techniques.[17] Design can be more complex and the need for head change limits the feasible actuation solutions. Rotational and translational-push actuation can be used while translational-pull (e.g., tendons) and translational-push-pull actuation can be hardly adopted (need to plug-unplug tendons/rods with problems of calibration and backlash).

Benefits of the modular needlescopic architecture are head interchangeability (few heads for a large set of instruments), easy sterilization of sticks, reduction of consumable parts, with economic benefit.

2.3. Haptic surgeon-system interface

Intuitive and easy control of the instrument is a basic requirement for good performance of the surgeon. In traditional open surgery the surgeon interacts directly with tissues and surgical instruments are naturally handled and maneuvered. With manual laparoscopic surgery the surgeon is asked to adapt to the viewpoint of handling sticks from outside the patient's body with reverse movements and mechanical interfaces (levers, tendons) to generate actions inside the patient like closing a grasper or tilting a wrist. In robotic MIS it is very common to have a micro wrist near to the tool tip, e.g., the tilting angles for the EndoWrist are π in both directions. Guiding such an instrument is difficult and requires a lot of practice. Introducing robotics in MIS where the tool is controlled via a haptic interface we can relieve the surgeon from the motion constraints by giving the feeling of guiding the tool directly, as if his hands were inside the patient's body.[18] This approach makes tool guidance more intuitive and helps therefore to avoid operational errors. Providing force feedback for all 6-DOF creates an even more realistic feeling and increases the surgeon's performance especially for grasping tasks.[19]

The haptic interface can go beyond the abilities of a human hand by filtering possible hand tremor and using motion scaling for very precise tool movements. Further the mechanical architecture of the proposed haptic master already reflects the laparoscopic motion constraints which simplifies the mapping from master to slave kinematics.

2.4. Surgical requirements

In a standard laparoscopic surgery generally 4 key holes are required:[20] one for scope, two for instruments manipulated by surgeon and one for surgical instrument handled by assisting nurse where required. In diagnostic and minor surgical procedures (gynecological) two or even one hole(s) could be sufficient when aided by MRI or Ultrasonography.[4] For accessibility workspace is created at surgical site by inflating with CO_2 provided through trocar at a safe pressure. Placement and number of trocar vary depending upon patient and kind of surgical procedure. In an ideal bimanual setup involving active and assisting instruments, instruments should be placed at equal azimuth angles along a semi circular line (about 160 to 180 mm long) centered at the projection of the target organ and with $\pi/3$ elevation angle.[21] This ideal inclination angle is achieved by inclining the operating table. The targeted site should be imaged from 75 mm to 150 mm at $\pi/2$ angle; so the scope should be at a right angle to the working plane of the target organ. The inter-port distance can range between 50 mm and 140 mm.[22] The angle between instruments should be around $\pi/3$. The workspace required to reach the full extent of the abdomen cavity, laterally and longitudinally, is $\pi/3$ and $\pi/2$ cone angle respectively.[23] Surgeons spend 95% of the time in a conical workspace with vertex angle of $\pi/3$. The extrusion of 100 mm is adequate.

Manually operated assisting tools are also commonly employed in addition to the tools operated by the robotic arm.[24]

Needlescopy is less traumatic to abdomen due to smaller tools and leaves smaller scars giving better cosmetic results. For the corresponding surgical procedures, setup in needlescopy is same as standard laparoscopy.[25] Since the surgical procedures are also evolving together with technological advancements in tools, 2 port needlescopy requiring two surgical tools and one scope is becoming more prevalent.[26] For this purpose an extrusion range of 60 mm can be considered sufficient.

Since the needlescopic tools are less than 3 mm in diameter (in some cases around 1 mm), they are delicate and bend easily with lateral forces necessitating avoidance of forceful maneuvers.[27] Their manipulation is not easy and requires greater care and attention when performing surgery. Also due to the smaller dimension, it is easy to cause damage to tissues. For this reason the forces that the environment transmits to the surgical instrument are much lower than the ones for laparoscopic surgery (reference values for laparoscopy can be found[28]) and they are dependant on the strength of the instrument.

Consequently forces and moments allowed by the standard needlescopic instruments for safe manipulation of the tissues were calculated jointly with MI surgeons from the S. Martino Hospital in Genoa and are given in Table I. In lateral manipulations (with displacement orthogonal to the

Table I. Bending stress and deflection of reference needlescopic instrument.

Outer Diameter	2 mm
Inner Diameter	1 mm
Bending Force	2.5 N
Distance instrument-tip – incision	150 mm
Bending Moment	370 Nmm
Bending Stress	500 N/mm²
Deflection of instrument tip	18 mm
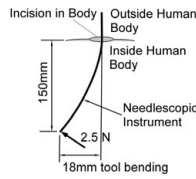
instrument) 2.5 N of equivalent force at instrument tip is considered as limit and it is more than adequate for general procedures. It should be noted that it causes quite a large instrument flexion of 18 mm. Resultant moments are M_x and M_y of 370 Nmm. Whereas, M_z is 50 Nmm for the offset of 20 mm between instrument tip and axis of the instrument. Similarly, axial force F_z equivalent to 2 N is considered adequate.

3. Development of the PMAR Lean Manipulation Module

The design of the lean manipulation module has been carried out in two steps from an original 4-DOF purely parallel architecture proposed for robotic laparoscopic surgery and used as reference starting point.

On the basis of the requirements for laparoscopic surgery a 4-DOF SP-equivalent purely parallel architecture is proposed[29] where feasibility checks comprise kinematics and singularities. A particular arrangement of the links exists such that no link collisions occur in the surgical workspace. The 4-DOF mechanism (Fig. 2a) comprises four legs with the same (RRR)R‖R architecture: three revolute joints (ξ_1^L, ξ_2^L, ξ_3^L for the generic L leg, $L = A, B, C, D$, counting from the base) with axes intersecting at the CPoR O common to all four legs and two parallel revolute joints (ξ_4^L, ξ_5^L) parallel to a tilting plane π_0 through O common to all legs; ξ_1^L is actuated. In each leg the first and second link from the base belong to the leg spherical submechanism while third and fourth links are for end-effector translation and belong to the heave submechanism.

A lean needlescopic manipulation module has been developed starting from this 4-DOF architecture. During the

design two problems were met: (a) although the surgical workspace is free of singularities and generally well-conditioned the actuation torque required to generate the goal tool force asks for electric motors big compared to the mechanism size and packaging becomes complex; (b) with the link arrangement avoiding collisions the mechanism becomes too large to satisfy the requirements on inter-port distance and angle between instruments (see Section 2.4), i.e., it is not possible to place more robots sufficiently close each other above the patient to handle the different surgical instruments.

The first problem can be overcome using actuators different from electrical motors also accordingly to the fact that the range of rotation is lower than π.

With reference to the second problem, more compact collision-free arrangements of the links have been studied but apart manufacturing complexity the curved link designs obtained could not provide sufficient stiffness. Limitations are on the lateral space occupied by the mechanism while there are no strict limitations on mechanism height orthogonally to the patient's body.

The arrangement proposed[28] to avoid collisions is with the spherical submechanisms of the legs moving on spheres with different radii with the radius of the internal sphere close to the distance between ξ_4^L and ξ_5^L. Consequently the lateral and vertical overall sizes of the mechanism are similar. Reducing the radii of the spheres results in collisions with the instrument which cannot be reasonably overcome by adopting curved link designs.

In conclusion the architecture[28] appears suitable for setups where only one robot is used, e.g., for diagnosis. A different architecture with lower number of links is necessary to achieve a collision-free design compact enough to place more robots sufficiently close each other on the patient's body to carry out multiple-instrument surgery.

The design steps are briefly reported to underline the relevance of size, design and packaging aspects in the development of MIS manipulators for needlescopic surgery.

3.1. Modified 2(RRR)P-2(RRR)R‖R architecture
The link collisions most difficult to overcome in the original 4-DOF mechanism are between the spherical and heave links
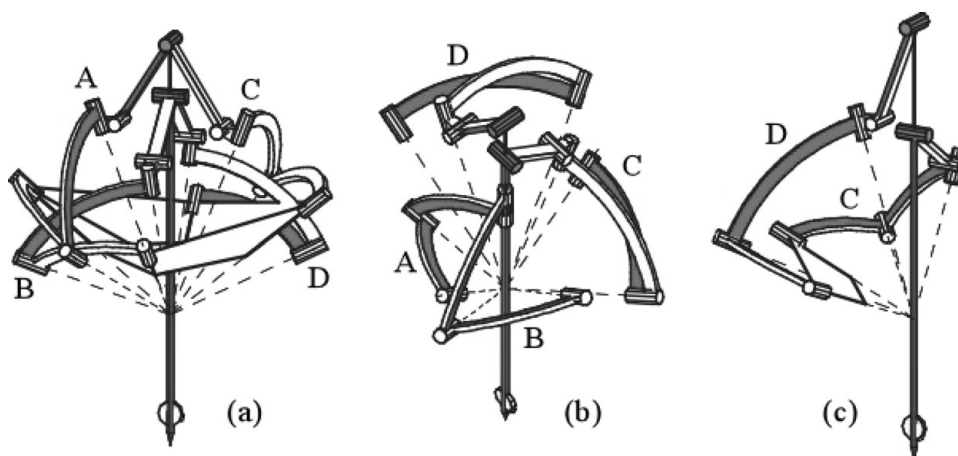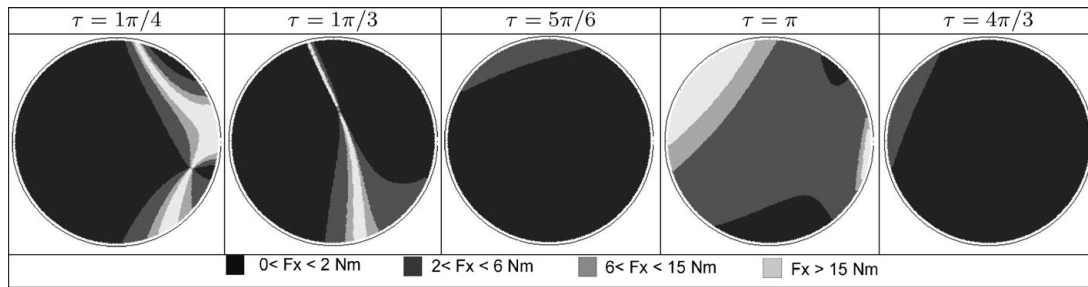

Fig. 2. SP-equivalent original purely parallel (a), modified (b), and final (c) slave surgical architectures.

Table II. Distribution of actuation torques in the workspace for given torsion values (equally spaced grid and fixed extrusion: tool at bottom most position).

$\tau = 1\pi/4$	$\tau = 1\pi/3$	$\tau = 5\pi/6$	$\tau = \pi$	$\tau = 4\pi/3$

■ $0 < Fx < 2$ Nm   ■ $2 < Fx < 6$ Nm   ■ $6 < Fx < 15$ Nm   ▫ $Fx > 15$ Nm

of different legs when the instrument is at one extremity of the torsion range. Hence the original 4-DOF mechanism has been modified replacing in two legs (say A and B) the heave submechanism with a P-joint parallel to the direction of extrusion (Fig. 2b). This is kinematically equivalent to have the fourth R-joint $\boldsymbol{\xi}_4^L$ of the leg at infinity with respect to O and not in the plane π_0.

The two P-joints of legs A and B can be also merged in one without changing the motion of the end-effector. The combined structural constraint applied by the series–parallel leg AB (equal to the sum of the constraints of legs A and B) is the same $\mathcal{W}_0 = \mathrm{Span}(\boldsymbol{\varphi}_x, \boldsymbol{\varphi}_y)$ applied by the four legs in the original 4-DOF mechanism; $\boldsymbol{\varphi}_x$ and $\boldsymbol{\varphi}_y$ are two pure forces through O in π_0 (orthogonal to the surgical instrument axis). With the actuated joints $\boldsymbol{\xi}_1^A$, $\boldsymbol{\xi}_1^B$ locked leg AB fixes the direction of the instrument. Legs C and D apply a redundant structural constraint belonging to $\mathcal{W}_0$ and they fix the end-effector torsion and extrusion when locking the actuated joints $\boldsymbol{\xi}_1^C$, $\boldsymbol{\xi}_1^D$.

Position and velocity kinematics of this mechanism are presented in ref. [30], a singularity free geometry is obtained and maps of the Jacobian conditioning discussed. The mechanism satisfies all functional requirements. Feasible link designs avoiding collisions in the whole workspace and satisfying the constraints on lateral space occupied by the mechanism have been worked out.

In the end problems were encountered related to actuation torques as shown by Table II. Plotted at constant extrusion (when tool is at lowermost position) for various values of torsion in the workspace, it is evident that actuation torques are very high and unavoidable distributed all-over the tilting workspace. The maximum actuation torque required to apply 2 N force along the axis of the instrument is greater then even 15 Nm. The same force can be applied with actuation torque of less then 2 Nm in other cases.

The mechanical reason is that external instrument extrusion/torsion forces/moments are balanced by components of the actuation moments of legs C and D only and these components are small in some workspace regions.

The requirements on maximum forces applied by the instrument are the same in the whole workspace hence it is not acceptable to size the actuators to provide the desired forces in the central workspace region and lower forces in the boundary region. Moreover it is assumed that the system can provide maximum forces continuously, thus actuators operating in transient conditions to provide extra torque for a limited amount of time are not acceptable.

The conclusion is that the actuators have to be sized for the worst transmission condition and this result in 6–15 times oversizing in approximately 40% of the workspace (for the best geometry found).

Because the overall size of the mechanism is a major constraint, this makes the architecture not fully suitable for the application. A further modification of the original architecture has been considered to deal with this short coming.

3.2. Final hybrid 2(RRR)R∥R architecture
End-effector torsion and extrusion can be constrained in the whole workspace with quite uniform actuation torques by locking the second revolute joints of the leg spherical submechanisms instead of the first ones. Two (RRR)R∥R legs (Fig. 2c) provide the complete combined structural and actuated constraint required and a collision-free mechanism is obtained with simple link designs and good force transmission in the whole workspace.

The use of a serial (RRR)P mechanism has been proposed and investigated.[31] The actuation of the third R-joint and of the P-joint is complex: motors directly connected to the joints occupy space making instrument connection complex; Transmissions introduce mechanical play and friction with problems of accuracy and control of forces applied by the instrument. These problems are solved using the second leg.

The following sections discuss modeling and functional performance of the mechanism.

3.2.1. Inverse position kinematics. The inverse position problem is solved as in the original 4-DOF mechanism. The extrusion and spherical subchains of the leg are considered separately. The pose of the instrument $[\mathbf{R}, h]$ is known, with $\mathbf{R}$ the instrument rotation matrix (tilt and torsion angles) and h measuring the extrusion.

For the extrusion subchain consider Fig. 3(a) and the generic leg $L = A, B$. We calculate $\mathbf{k}_3^L$. The instrument reference frame is used with $\mathbf{k}_o$ through O along the instrument and $\mathbf{i}_o$ in π^A. The triangle $O P_5^L P_4^L$ is a virtual 1-DOF mechanism with parameter $H^L = h + h^L$. By trigonometric considerations we obtain for $c_4^L = \cos \psi_4^L$ and $s_4^L = \sin \psi_4^L$ the equation: $2r_4^L H^L c_4^L + 2r_4^L r_5^L s_4^L - H^{L^2} - N^L = 0$ where $N^L = r_5^{L^2} + r_4^{L^2} - l_{45}^{L^2}$. All parameters are
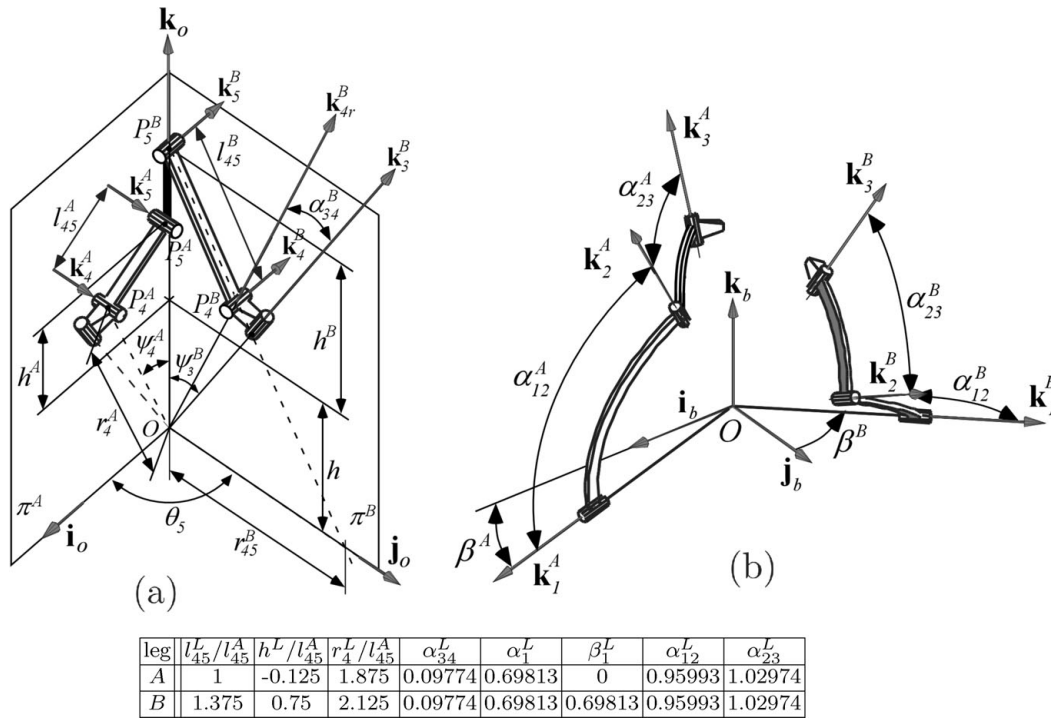
Fig. 3. Geometry parameters for heave (a) and spherical (b) submechanisms and table with the adopted values.

leg	l_{45}^L/l_{45}^A	h^L/l_{45}^A	r_4^L/l_{45}^A	α_{34}^L	α_1^L	β_1^L	α_{12}^L	α_{23}^L
A	1	-0.125	1.875	0.09774	0.69813	0	0.95993	1.02974
B	1.375	0.75	2.125	0.09774	0.69813	0.69813	0.95993	1.02974

shown in Fig. 3. The solutions are

$$\begin{bmatrix} c_4^L \\ s_4^L \end{bmatrix} = \frac{1}{2r_4^L\left(H^{L2}+r_5^{L2}\right)} \begin{bmatrix} H^L & -r_5^L \\ r_5^L & H^L \end{bmatrix} \begin{bmatrix} H^{L2}+N^L \\ \varepsilon^L C_\varepsilon^L \end{bmatrix},$$
(1)

where $\varepsilon^L = \pm 1$ distinguishes between the two feasible working modes of the triangle $OP_5^L P_4^L$, $C_\varepsilon^L = \sqrt{-(H^{L2}-m_H^L)(H^{L2}-M_H^L)}$, $M_H^L=(r_4^L+l_{45}^L)^2-r_5^{L2}$ and $m_H^L=(r_4^L-l_{45}^L)^2-r_5^{L2}$; $m_H^L \le H^{L2} \le M_H^L$.

$\mathbf{k}_4^A = \mathbf{j}_o$ and $\mathbf{k}_4^B = \mathbf{R}_z(\theta)\,\mathbf{j}_o$ with $\mathbf{R}_z(\theta)$ rotation matrix about $\mathbf{k}_o$. Analogously $\mathbf{k}_{4r}^A = [s_4^A, 0, c_4^A]^T$, $\mathbf{k}_{4r}^B = \mathbf{R}_z(\theta)\,[s_4^B, 0, c_4^B]^T$.

$\mathbf{k}_3^L$ is obtained rotating $\mathbf{k}_{4r}^L$ of an angle α_{34}^L about $\mathbf{k}_4^L$.

The distance r_{45}^L from O of the intersection between π_0 and π_{45}^L is $r_{45}^L=(p^L \varepsilon^L C_\varepsilon^L)((p^L - r_4^{L2} + l_{45}^{L2})\,H^L)^{-1}$, with $p^L = H^{L2}+r_5^{L2}$.

For the spherical subchain consider Fig. 3(b). $\mathbf{k}_1^L = \mathbf{R}\,\mathbf{k}_{1b}^L$ is calculated from $\mathbf{k}_{1b}^L$ expressed in the base frame and $\mathbf{k}_2^L$ is calculated from $\mathbf{k}_1^L$ and $\mathbf{k}_3^L$:

$$\mathbf{k}_2^L = \left(t_1^L\,\mathbf{k}_1^L + t_2^L\,\mathbf{k}_3^L + t_3^L\,\mathbf{k}_1^L \times \mathbf{k}_3^L\right)\left(1-c_{13}^{L2}\right)^{-1},$$

with

$$c_{13}^L = \mathbf{k}_1^L \cdot \mathbf{k}_3^L, \quad t_1^L = c_{12}^L - c_{23}^L c_{13}^L, \quad t_2^L = c_{23}^L - c_{12}^L c_{13}^L,$$

$$t_3^L = \delta^L C_\delta^L, \quad C_\delta^L = \sqrt{-(c_{13}^L - m_S^L)(c_{13}^L - M_S^L)},$$

$$m_S^L = c_{12}^L c_{23}^L - |s_{12}^L s_{23}^L|, \quad M_S^L = c_{12}^L c_{23}^L + |s_{12}^L s_{23}^L|,$$

$$c_{ij}^L = \cos\alpha_{ij}^L, \quad s_{ij}^L = \sin\alpha_{ij}^L.$$

The boolean parameter $\delta^L = \pm 1$ distinguishes between the two working modes of the spherical subchain of leg L.

The actuation angles θ_1^L and θ_2^L are easily computed from $\mathbf{k}_1^L, \mathbf{k}_2^L, \mathbf{k}_3^L$.

3.2.2. Forward position kinematics. The forward position problem reduces to the calculation of the instrument pose from $\mathbf{k}_3^A$ and $\mathbf{k}_3^B$, which are immediately available when assigned the actuation angles.

The instrument axis has the unknown direction $\mathbf{k}_o$. $\mathbf{k}_o$ can be expressed as a linear combination of $\mathbf{k}_3^A, \mathbf{k}_3^B, \mathbf{k}_3^A \times \mathbf{k}_3^B$ as for $\mathbf{k}_2^L$ in the inverse position problem:

$$\mathbf{k}_o = \left(t_1\mathbf{k}_3^A + t_2\mathbf{k}_3^B + t_3\mathbf{k}_3^A \times \mathbf{k}_3^B\right)\left(1-c_3^{AB2}\right)^{-1}$$

The coefficients t_1, t_2, t_3 are calculated from three equations stating that (Eq. I) the distance and (Eq. II) the angle between the R-joints on the instrument are respectively the geometry parameters $H^A - H^B$ and θ_5; (Eq. III) $\mathbf{k}_o$ has unit length.

To single out EqI consider the heave submechanism of leg $L = A, B$ in the plane π^L through O parallel to $\mathbf{k}_3^L$ and $\mathbf{k}_o$ (Fig. 3a). H^L is related to t_1 and t_2 by the equation:

$$H^{L2} + r_4^{L2} - 2r_4^L H^L c_{34}^L T^L - 2r_4^L H^L B_1^L$$
$$\times \sqrt{c_{34}^{L2} T^{L2} - T^{L2} + s_{34}^{L2}} - l_{45}^{L2} = 0 \quad (2)$$

with $T^A = t_1 + t_2 p^{AB}$, $T^B = t_1 p^{AB} + t_2$, $p^{AB} = \mathbf{k}_3^A \cdot \mathbf{k}_3^B$, $B_1^L = \pm 1$ boolean parameter distinguishing between two assembly modes of the heave submechanism. Note that t_3 does not appear.

Equation (2) can be solved in H^L introducing the boolean parameter $B_2^L = \pm 1$ which distinguishes between the other

two assembly modes of the heave submechanism. Eq. I is obtained as $(H^A - H^B)^2 = H^2$ with H geometry parameter known.

With $\pi_{34}^L = 0$ or $\pi_{34}^L = \pi/2$ the expressions of H^L (and consequently Eq. I) simplify remarkably obtaining respectively:

$$r_4^L T^L + B_2^L \sqrt{r_4^{L\,2} T^{L\,2} - r_4^{L\,2} + l_{45}^{L\,2}}$$

and

$$r_4^L B_1^L \sqrt{1 - T^L} + B_2^{L\,2} \sqrt{-r_4^{L\,2} T^{L\,2} + l_{45}^{L\,2}},$$

which further simplify if $l_{45}^L = r_4^L$.

Eq. III clinical experience of needle-laparoscopic calculated as $\mathbf{k}_o^{\,2} = 1$ gives t_3 as a function of t_1 and t_2: $t_3^2 = (t_1^2 + 2t_1 t_2 p_3^{AB} + t_2^2 - 1)/(-1 + p^{AB\,2})$.

Eq. II is calculated as $(\mathbf{k}_3^A \times \mathbf{k}_o) \cdot (\mathbf{k}_3^B \times \mathbf{k}_o) - c_5 = 0$, $c_5 = \cos\theta_5$. Substituting t_3 obtained from Eq. III and simplifying gives: $p^{AB} - T^A T^B - c_5 = 0$.

Eq. I and Eq. III can be solved in T^A and T^B from which t_1 and t_2 are immediately calculated. An analytical parametric solution is difficult to obtain in the general case apart for $\pi_{34}^L = 0$ or $\pi/2$. t_3 is calculated from t_1 and t_2 by substitution and finally $\mathbf{k}_o$ is obtained. h can be calculated from one of Eq. (2). The torsion angle is immediately calculated from $\mathbf{k}_3^A$, $\mathbf{k}_3^B$, $\mathbf{k}_o$.

3.2.3. Velocity kinematics.

We use the rotating reference frame $O\mathbf{i}_o\mathbf{j}_o\mathbf{k}_o$ for ease and apply the method detailed in ref. [16]. The input-output velocity equations are: $[\mathbf{Z}_a\ \mathbf{Z}_c]^T \boldsymbol{\xi} = [\boldsymbol{\Lambda}\dot{\boldsymbol{\theta}}_a\ \mathbf{0}_2]^T$, where, out of singularities, $\mathbf{Z}_a = [\tilde{\boldsymbol{\varphi}}_1^A\ \tilde{\boldsymbol{\varphi}}_2^A\ \tilde{\boldsymbol{\varphi}}_1^B\ \tilde{\boldsymbol{\varphi}}_2^B]^T$, $\mathbf{Z}_c = [\tilde{\boldsymbol{\varphi}}_x\ \tilde{\boldsymbol{\varphi}}_y]^T$ (with the symbol $\sim$ on a wrench denoting switching of force and moment components), $\boldsymbol{\Lambda} = \mathrm{diag}\{\boldsymbol{\varphi}_1^A \circ \boldsymbol{\xi}_1^A, \boldsymbol{\varphi}_2^A \circ \boldsymbol{\xi}_2^A, \boldsymbol{\varphi}_1^B \circ \boldsymbol{\xi}_1^B, \boldsymbol{\varphi}_2^B \circ \boldsymbol{\xi}_2^B\}$.

The different entries of $\mathbf{Z}_a$ and $\boldsymbol{\Lambda}$ can be calculated using the geometry of the mechanism. In $O\mathbf{i}_o\mathbf{j}_o\mathbf{k}_o$, the $\mathbf{i}_o$ and $\mathbf{j}_o$ components of the translation velocity are always zero due to $\mathcal{W}_0$ and we can consider the simplified end-effector twist $\bar{\boldsymbol{\xi}}$ with the only three rotational and $\mathbf{k}_o$ translational components. So, the simplified velocity equation, $\mathbf{Z}\boldsymbol{\xi} = \boldsymbol{\Lambda}\dot{\boldsymbol{\theta}}$, considering the screws reciprocal to all except the actuated screws for each case of actuation, can be expressed as following:

$$\begin{bmatrix} (\mathbf{k}_2^A \times \mathbf{k}_3^A)^T & \dfrac{k_2^A k_3^A k_4^A}{-r_{45}^A} \\ (\mathbf{k}_1^A \times \mathbf{k}_3^A)^T & \dfrac{k_1^A k_3^A k_4^A}{-r_{45}^A} \\ (\mathbf{k}_2^B \times \mathbf{k}_3^B)^T & \dfrac{k_2^B k_3^B k_4^B}{-r_{45}^B} \\ (\mathbf{k}_1^B \times \mathbf{k}_3^B)^T & \dfrac{k_1^B k_3^B k_4^B}{-r_{45}^B} \end{bmatrix} \bar{\boldsymbol{\xi}}$$

$$= \begin{bmatrix} \mathbf{k}_1^A \mathbf{k}_2^A \mathbf{k}_3^A & 0 & 0 & 0 \\ 0 & \mathbf{k}_2^A \mathbf{k}_1^A \mathbf{k}_3^A & 0 & 0 \\ 0 & 0 & \mathbf{k}_1^B \mathbf{k}_2^B \mathbf{k}_3^B & 0 \\ 0 & 0 & 0 & \mathbf{k}_2^B \mathbf{k}_1^B \mathbf{k}_3^B \end{bmatrix} \begin{bmatrix} \dot{\theta}_1^A \\ \dot{\theta}_2^A \\ \dot{\theta}_1^B \\ \dot{\theta}_2^B \end{bmatrix}, \tag{3}$$

where r_{45}^L in leg $L = A, B$ is the distance between $\pi_{45}^L \cap \pi_0$ and O. From the above equation, end-effector velocities can be obtained if actuator rotational velocities are known, and similarly vice versa.

3.2.4. Jacobian conditioning and geometry.

Redundant output (RO) and Redundant Passive Motion (RPM) singularities were searched through the desired workspace using a C++ code. Checks for RO were based on the conditioning of the forward Jacobian matrix expressed as $J_F = \mathbf{Z}^{-1}\boldsymbol{\Lambda}$. Frobenious Norm was used as conditioning criterion. Color maps were generated to highlight the surfaces of singularity in the workspace. Results for some workspace sections (at constant h and torsion) for the torsional and extrusion range are shown in Table III. White colors represent singular configurations while colors from light gray to dark gray show conditioning of the matrices. As the entries of matrix $\mathbf{Z}$ are nonhomogeneous, the conditioning only determines the presence or absence of singularities. Since the analysis performed is at discrete locations it is not proven that no singularity exists in the workspace between the examined configurations but the grid of configurations examined is very dense.

As a result of the kinematics and singularity analysis carried out the best set of geometric parameters achieved is shown in Fig. 3. The corresponding singularity free workspace is a truncated cone with half angle $13\pi/90$ and extrusion range 86 mm which is even suitable for standard laparoscopic procedures. Whereas the torsional range of the mechanism from singularity point of view is more than $3\pi/2$. Since all the links are mobilized to provide the movements including torsional, the mechanism topology imposes a hinderance to achieve such a large torsional workspace due to the issue of some of the links crossing with the surgical instrument.

3.2.5. Sizing of actuators and packaging.

Static analysis was performed to ensure that the manipulator is able to provide the forces and torques required at the surgical tool with actuators of reasonable size for compact packaging of the components.

The actuator torques $\boldsymbol{\tau}$ are computed from given external forces and moments $\mathbf{F}$ at the surgical instrument using relation $\boldsymbol{\tau} = \mathbf{J_F}^{-T}\mathbf{F}$. Whole workspace was scanned at constant extrusion, incrementing tilt and torsion angles sequentially, employing the maximum moments and force expected at the surgical instrument (see Section 2.4). The maximum actuators torques obtained are shown in Tab. IV. The extrusion value of the surgical tool for the plotted results was selected to be such that the tool is at bottom most position; as for this architecture, this position was found to be requiring maximum actuator torques. For the ideal case highest torque expected from actuator is around 2 Nm. Consequently, after including the effect of friction at joints and at the keyhole, play-free actuators matching the desired overall size of the system can be adopted and the system can be fully packaged as shown in the Fig. 4.

Table III. Conformal conditioning maps (the smaller the darker) for given
extrusion and torsion – no singularities are present.

Extrusion h^A	$\tau = 1\pi/4$	$\tau = 1\pi/2$	$\tau = 3\pi/4$	$\tau = \pi$	$\tau = 5\pi/4$
$(1.75)\, l_{45}^A$					
$(2.0)\, l_{45}^A$					
$(2.25)\, l_{45}^A$					
$(2.5)\, l_{45}^A$					

4. The PMAR Master
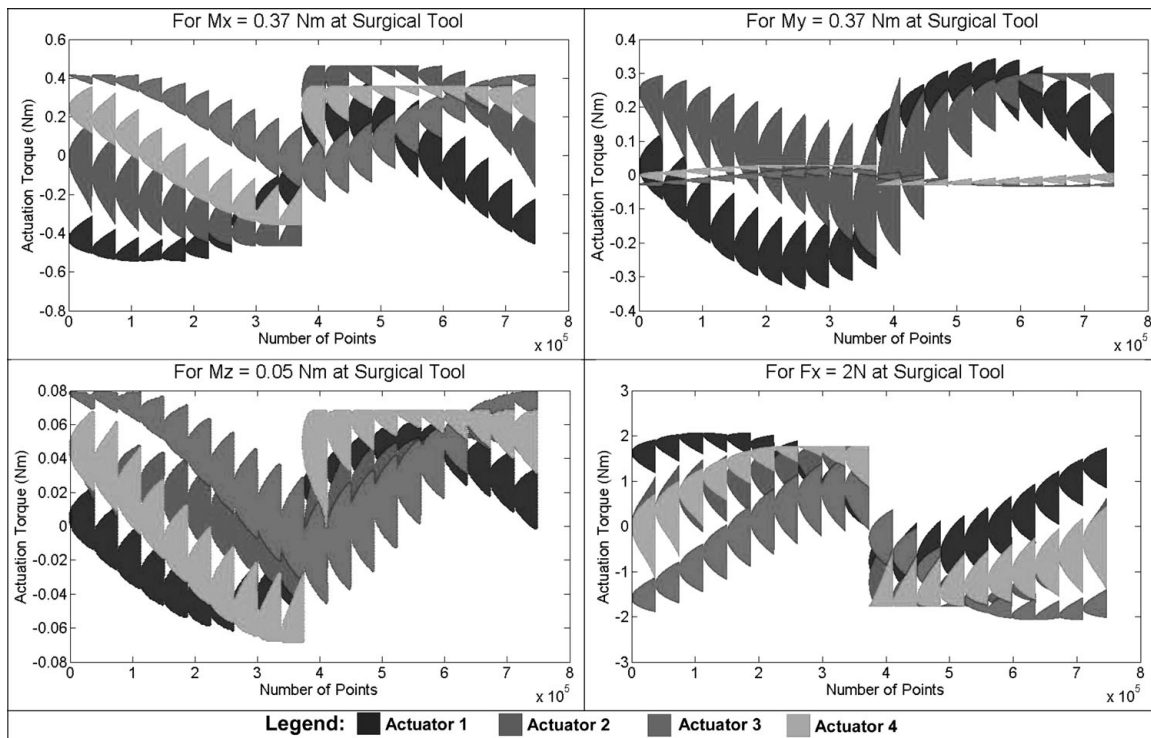
4.1. The proposed architecture

For the design of the haptic master, standard requirements for haptic interfaces have to be taken into account: minimum backdrive friction and backdrive inertia are crucial for accurate force feedback; high mechanical stiffness for large system bandwidth and minimum backlash are important as well.[32]

The selected architecture [3(RRR)][2P(RR)S-1P(RR)] is shown in Fig. 5. It appears correct to realize the rotation around the keyhole by a spherical submechanism. The parallel structure allows to place the actuated joints in the base in order to keep the inertia low. All the revolute joint axes intersect at the center point of rotation (CPR). Three prismatic joints are fixed on the movable base. One of them intersects with the CPR and is connected by a Cardanic joint to the handle which reflects the translational movement along the trocar. The other two legs are connected with the small platform of the handle by (RR)S-rods which allows tilting in two directions.

Each leg has its own motion plane avoiding leg collisions. The second links are all bent to avoid intersections with the joints on the movable platform. The advantage of this

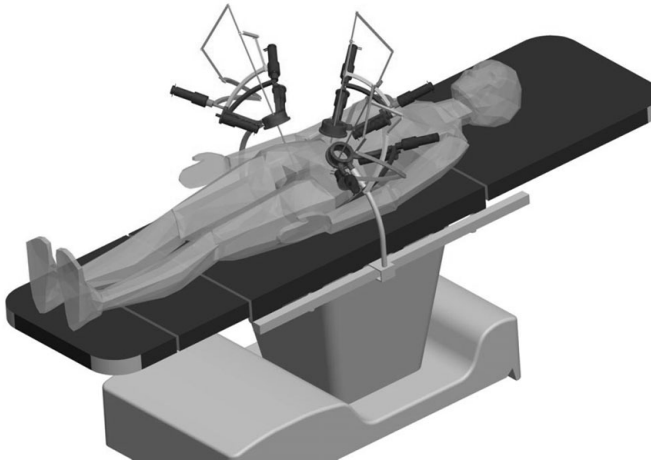Table IV. Actuators torques for peak force and moments applied at surgical tool.

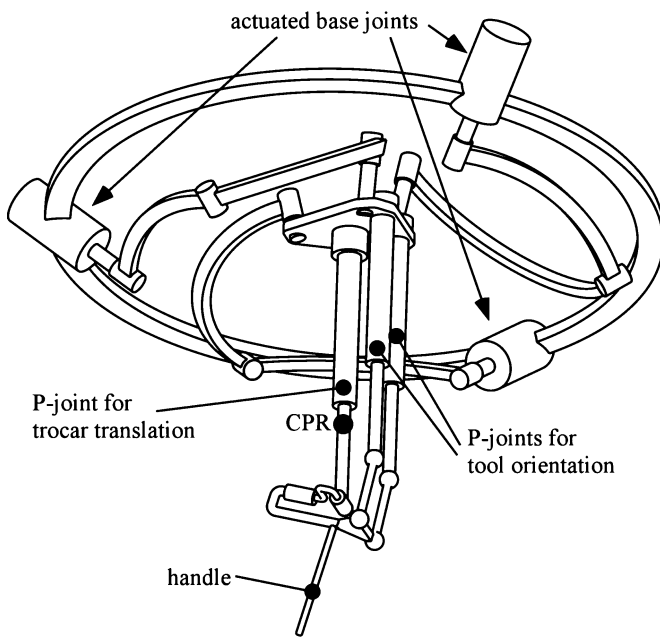Fig. 4. Surgical setup with 3 PMAR manipulation modules.

Fig. 5. Proposed architecture for the PMAR haptic master.

architecture is that all environmental constraints are already integrated in the mechanical architecture and the mapping of master position and orientation to the slave robot is quite direct. Further three actuators are fixed in the base which

reduces the inertia and the parallel structure guaranties high stiffness and low backlash which is important for accurate force feedback.

4.2. Geometry
The proposed architecture consists of two submechanisms, the spherical and the wrist submechanism. We define a global reference frame $O\mathbf{i}_b\mathbf{j}_b\mathbf{k}_b$ located in the CPR. The three actuated revolute joints are placed symmetrically around $\mathbf{k}_b$ with the first joint axis $\mathbf{k}_1^1$ lying in the plane spanned by $\mathbf{k}_o$ and $\mathbf{i}_o$ (Fig. 6a). The joint axes of the spherical mechanism are called $\mathbf{k}_i^L$ with L = A,B,C for the three legs and i the joint number starting by the fixed joint. The tilting angle θ is defined as the angle between the actuated joint axis $\mathbf{k}_1^L$ and $\mathbf{k}_o$. Further the link angles are defined as α_{12}^L and α_{23}^L. A second frame $O\mathbf{i}_o\mathbf{j}_o\mathbf{k}_o$ is attached to the wrist mechanism and located in the CPR with $\mathbf{k}_o$ aligned with the prismatic joint located in P^D (Fig. 6b). The joint axes $\mathbf{k}_3^L$, attached to the movable platform are arranged symmetrically with a tilting angle λ^L between its axis and $\mathbf{k}_o$. Finally the end-effector orientation is defined by frame $P\mathbf{i}_p\mathbf{j}_p\mathbf{k}_p$ with its y-axis aligned with the revolute joint fixed on the small platform. In zero-tilting position of the wrist submechanism the axis of frame $O\mathbf{i}_o\mathbf{j}_o\mathbf{k}_o$ and $P\mathbf{i}_p\mathbf{j}_p\mathbf{k}_p$ are parallel. The handle is in direction of $\mathbf{k}_p$.

4.3. Inverse kinematics
For the computation of the inverse kinematics both submechanisms can be considered nearly separately. The end-effector position and orientation is fully defined by its position coordinates, the torsion angle around the trocar axis (represented by $\mathbf{k}_p$) and the two tilting angles of the micro-wrist. We use tilt and torsion angles (T&T)[33] for describing the rotation of frame $O\mathbf{i}_o\mathbf{j}_o\mathbf{k}_o$ with respect to frame $P\mathbf{i}_p\mathbf{j}_p\mathbf{k}_p$. In this way it is possible to define explicitly the torsion around the trocar. Knowing the position of the coordinates the prismatic joint length l^D is already defined. Transforming the end-effector position into T&T angles defines the orientation of frame $O\mathbf{i}_o\mathbf{j}_o\mathbf{k}_o$ and thus the orientation of the joint axis $\mathbf{k}_3^L$. Now we can obtain the orientation of the second joint axis in each leg $\mathbf{k}_2^L$ as a linear combination of $\mathbf{k}_1^L$ and $\mathbf{k}_3^L$. The orientation of the end-effector with respect to frame $O\mathbf{i}_o\mathbf{j}_o\mathbf{k}_o$ is defined by the two tilting angles ψ_1 and ψ_2. The joint variables l^E and l^F are computed with the following

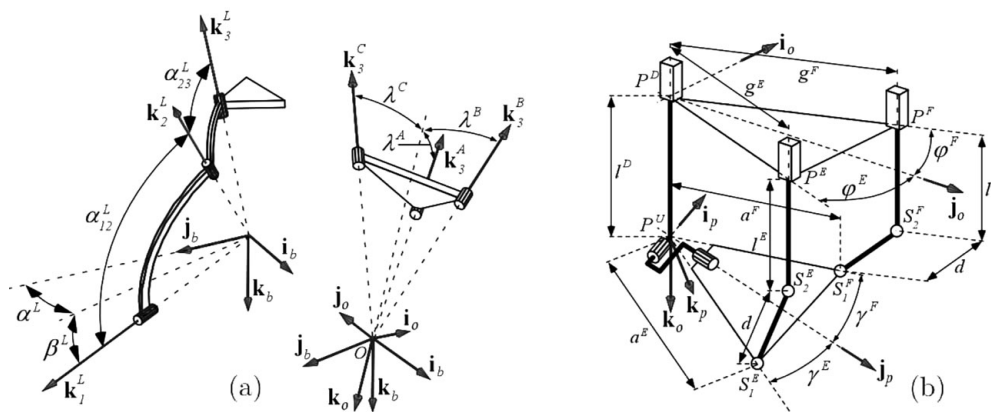

Fig. 6. Geometry of the spherical (a) and wrist (b) submechanism.

constraint: point S_2^L has to lie on a sphere around S_1^L with radius d.

$$l^L = \pm\sqrt{d^2 - \left(S_{2\mathbf{i}_o}^L - S_{1\mathbf{i}_o}^L\right)^2 - \left(S_{2\mathbf{j}_o}^L - S_{1\mathbf{j}_o}^L\right)^2} + S_{1\mathbf{k}_o}.$$
$$L = E, F \tag{4}$$

4.4. Velocity kinematics

Accordingly to ref. [16] for each submechanism we distinguish a system of structural constraints and a system of actuated constraints of dimensions 3 and 6 respectively representing the combined constraint applied by the legs to the end-effector when all joints are free and the actuated joints are locked respectively. We can single out a base of three wrenches for the system of structural constraints and three actuated constraint wrenches completing to 6 the base of the system of structural constraints.

Consider the spherical submechanism. The system of structural constraints is $\mathcal{W}^s = \{\boldsymbol{\zeta}_c^{sL} \mid L = A, B, C\}$ containing all pure forces through the CPR. For each leg the actuated constraint wrench $\boldsymbol{\zeta}_a^{sL}$, $L = A, B, C$, is a pure moment $\boldsymbol{\mu}_a^{sL}$ in direction $\mathbf{k}_2^L \times \mathbf{k}_3^L$.

Consider now the wrist submechanism. The system of structural constraints is $\mathcal{W}^w = \boldsymbol{\zeta}\{\boldsymbol{\zeta}_c^{wL} \mid L = A, B, C\} = \{\boldsymbol{\varphi}_c^{w1}, \boldsymbol{\varphi}_c^{w2}, \boldsymbol{\mu}_c^w\}$ spanned by two pure forces $(\boldsymbol{\varphi}_c^{w1}, \boldsymbol{\varphi}_c^{w2})$ orthogonal each other and to $\mathbf{k}_o$ with $\boldsymbol{\varphi}_c^{w1}$ parallel to $\mathbf{i}_o$ and by the pure moment $\boldsymbol{\mu}_c^w$ in direction $\mathbf{i}_o \times \mathbf{j}_p$. The actuated constraint wrenches $\boldsymbol{\zeta}_a^w$ are: a pure force $\boldsymbol{\varphi}_a^{w1}$ parallel to $\mathbf{k}_o$, the pure forces $\boldsymbol{\varphi}_a^{w2}$ through points S_1^E, S_2^E and $\boldsymbol{\varphi}_a^{w3}$ through S_1^F, S_2^F.

In general for a PPM taking the reciprocal product of the end-effector twist $\boldsymbol{\xi} = (\boldsymbol{\omega} \mid \mathbf{v})^T$ and the reciprocal screws that form the basis of $\mathcal{W}$ and $\mathcal{V}$ yields

$$\boldsymbol{\zeta}_{cj} \circ \boldsymbol{\xi} = 0 \quad j = 1 \ldots 6 - n \tag{5}$$

$$\boldsymbol{\zeta}_{aj} \circ \boldsymbol{\xi} = \sum_{i=1}^{n} \dot{\theta}_i \boldsymbol{\zeta}_i \quad j = 1 \ldots n \tag{6}$$

where the $\boldsymbol{\zeta}_{cj}$ are a base of $\mathcal{W}$ and the $\boldsymbol{\zeta}_{aj}$ complete $\mathcal{W}$ to $\mathcal{V}$. In matrix form Eq. (5) is $\mathbf{Z}_c \boldsymbol{\xi} = 0$ where $\mathbf{Z}_c = [\tilde{\boldsymbol{\zeta}}_{c1}^T \ldots \tilde{\boldsymbol{\zeta}}_{c,6-n}^T]^T$ and we denote $\tilde{\boldsymbol{\zeta}}^T = (\mathbf{m}^T \mid \mathbf{f}^T)$. Equation (6) is in matrix form $\mathbf{Z}_a \boldsymbol{\xi} = \boldsymbol{\Lambda} \dot{\boldsymbol{\theta}}$, where $\mathbf{Z}_a = [\tilde{\boldsymbol{\zeta}}_{a1}^T \ldots \tilde{\boldsymbol{\zeta}}_{an}^T]^T$ and $\boldsymbol{\Lambda} = \text{diag}(\boldsymbol{\Lambda}_1 \ldots \boldsymbol{\Lambda}_n)$. Each diagonal block has the element $\boldsymbol{\Lambda}_i = \boldsymbol{\zeta}_{ai} \circ \boldsymbol{\xi}_{ai}$, $i = 1 \ldots n$ with $\boldsymbol{\xi}_{ai}$ as the screw axis of the actuated joint i with the respective joint velocity $\dot{\theta}_i$. The matrix of constraints $\mathbf{Z}_c$ and the matrix of actuation $\mathbf{Z}_a$ can be combined as

$$\begin{bmatrix} \mathbf{Z}_a \\ \mathbf{Z}_c \end{bmatrix} \boldsymbol{\xi} = \begin{bmatrix} \boldsymbol{\Lambda} & \mathbf{0} \\ \mathbf{0} & \mathbf{I}_{6-n} \end{bmatrix} \begin{bmatrix} \dot{\boldsymbol{\theta}} \\ \mathbf{0}_{6-n} \end{bmatrix}. \tag{7}$$

In configurations away from singularities the combined Z-matrix has full rank and is therefore invertible. Now the overall output twist of the entire mechanism can be obtained by summing up the twists of both submechanisms: $\boldsymbol{\xi} = \boldsymbol{\xi}^s + \boldsymbol{\xi}^w = \mathbf{J}^{-1}[\dot{\boldsymbol{\theta}}^s \, \dot{\boldsymbol{\theta}}^w]^T$, where the inverse Jacobian $\mathbf{J}^{-1}$ consists of the first three columns of $\mathbf{J}_s^{-1}$ and $\mathbf{J}_w^{-1}$ (the inverse Jacobians of spherical and wrist submechanisms).

4.5. Dexterity analysis

As for the inverse kinematics, the dexterity analysis is performed in two steps. First, we check if the spherical submechanism can provide all required orientations and secondly if the wrist submechanism can offer enough tilting for the microwrist. As dexterity criterion we chose the condition number c based on Frobenius norm: $c(J) = \|\boldsymbol{J}\| \|\boldsymbol{J}^{-1}\|$ with $\|A\| = \sqrt{\sum_{i,j} a_{i,j}^2}$.

A condition number of one means that the mechanism is perfectly conditioned, whereas a condition number rising to infinity intends a configuration close to singularity. We use the results of the dexterity analysis for choosing the geometrical parameters, which will then be verified by static force analysis.

Consider the spherical submechanism. Obvious singular configurations can be avoided by choosing appropriate geometrical parameters. Different link angles δ_{12} and δ_{23} avoid aligned joint axis $\boldsymbol{k}_1^L$, $\boldsymbol{k}_3^L$ and also stretched legs can be avoided easily. In general it turned out that a big tilting angle θ enlarged the well conditioned workspace, but in order to assure enough free space for the surgeon's hand we defined the constraint that the second joint of each leg should not cross the zero plane spanned by $\mathbf{i}_b$ and $\mathbf{j}_b$. The size of the movable platform depends on the distance between the prismatic joints. In general enlarging this distance yields a better conditioning, but requires also longer (RR)S-rods. This is contrary to the objective of keeping the sphere radius r small, because the prismatic joints must be placed inside the sphere. The outer planes are already occupied by the moving legs. Finally, the chosen geometrical parameters are a compromise between a well conditioned workspace and a small size of the mechanism. We use the parameters $r = 250$ mm, $\lambda^L = 7\pi/90$, $\theta = 17\pi/60$, $\alpha_{12}^L = 5\pi/18$, $\alpha_{23}^L = 23\pi/90$ for the spherical submechanism and $a^E = a^F = 45$ mm, $\gamma^E = \gamma^F = 2\pi/9$, $g^E = g^F = 50$ mm, $\varphi^E = \varphi^F = 7\pi/36$, $d = 65$ mm for the wrist submechanism. The results are shown in Fig. 7. For the spherical mechanism we checked all points in the workspace with a maximum vertex angle of $\pi/3$. It turned out that the conditioning of the spherical submechanism depends mainly on the torsion angle. As can be seen in Fig. 7(a) the conditioning is very good for torsion angles around $\pi/2$ but becomes worse for torsion angles beyond $\pi/15$ and $43\pi/45$ respectively. The sphere shown in Fig. 7(b) shows all the points the handle is pointing on for different tilting angles ψ_1 and ψ_2. We varied ψ_1 from $-\pi/5$ to $7\pi/15$ and ψ_2 from $-\pi/3$ to $\pi/3$. Especially in the two darker areas of the sphere for ψ_1 around $-1/5\pi$, ψ_2 around $1/3\pi$ the Jacobian becomes bad conditioned. These areas can be avoided by a smaller workspace and motion scaling in order to simulate the required tilting angles.

4.6. Static forces

The static model describes the relationship between torques or forces applied to the end-effector and the resulting joint torques. Using the principle of virtual work the external forces and the joint torques are mapped by the inverse transposed Jacobian $\boldsymbol{\tau} = \mathbf{J_F}^{-T}\mathbf{F}$ as in Section 3.2.5.
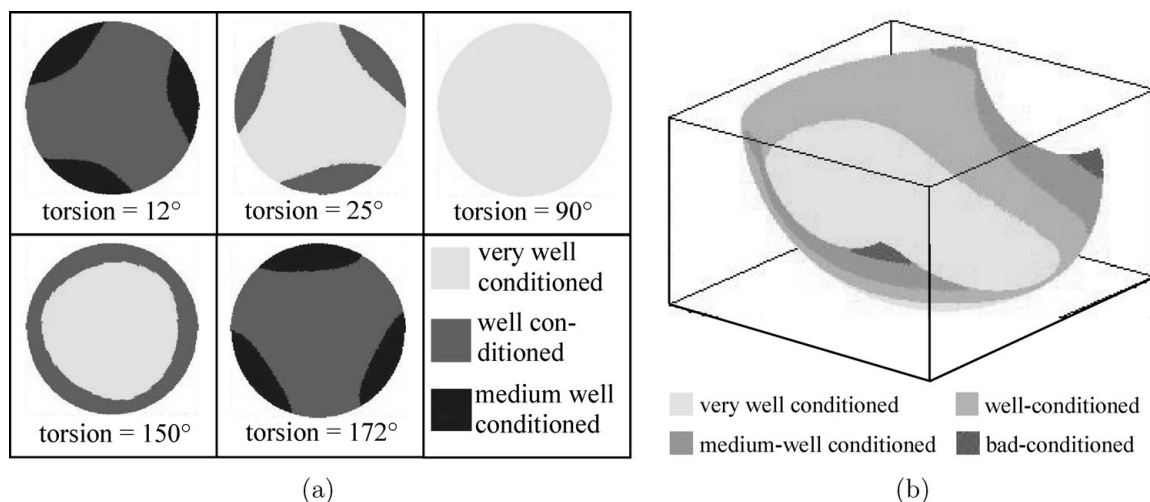
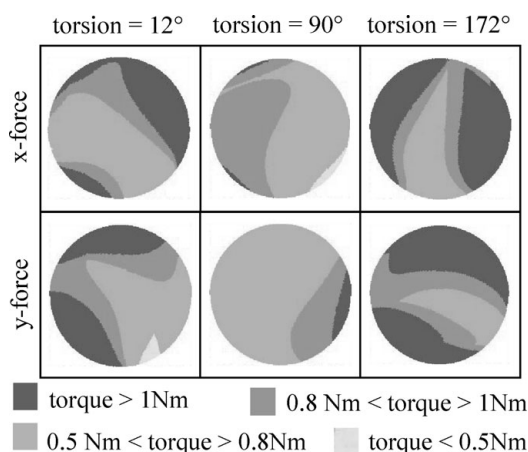Fig. 7. Dexterity Analysis for the spherical (a) and wrist submechanism (b).

Fig. 8. Joint torques of the spherical submechanism.

5. Conclusions

The paper proposes the new paradigm of lean robotic MIS system and discusses the development of a lean system for needlescopic surgery. Lean MIS systems are modular and scalable and can be customized to carry out specific sets of procedures. This may promote an increase in the number of procedures carried out with robotic MIS instead of standard manual practice with benefit for the patients.

The lean needlescopic system presented, dedicated to a wide field of abdominal operations, is developed at the PMAR lab of University of Genoa. Its basic modules are the guiding master and operating slave manipulators. For both, requirements and architectures are introduced discussing constraints and motivations. The mathematical models used during design and virtual prototyping are presented. They will be also used in the control system with the aim of improving the surgeon feeling all along the procedures and instrument performance.

The realization of the new lean surgical robotic modules is ongoing and a wide test campaign is planned to assess their effectiveness and robustness.

According to ref. [34] 11 N should be enough in order to simulate a rigid body in virtual environment. The objects touched by the surgeon using the operations are mainly compliant so that we suppose that 5 N should be enough feedback force. The objective is not to reflect the real forces, but to provide a force range large enough to make it easy for the surgeon to distinguish between different objects. We apply 5 N to the handle at a distance of 100 mm from the center of the cardanic joint, which reflects the way the surgeon grasps the handle. The force is applied in $\mathbf{i}_p$, $\mathbf{j}_p$ and $\mathbf{k}_p$ direction consecutively. The extrusion is fixed at 200 mm in order to have maximum torque around the CPR. The results for the spherical submechanism are shown in Fig. 8. For every configuration the highest of the three joint torques is checked and shown as gray-scaled areas. Areas with higher joint forces correlate with medium well-conditioned configurations. But even in those areas the maximum joint torques do not exceed 4 Nm. Considering the wrist mechanism it turned out that the force direction did not influence a lot the maximum joint forces. But areas of high forces correspond to bad conditioned areas, where the maximum forces do not exceed 26 N.

References
1. F. Cepolina, B. Challacombe and R. C. Michelini, "Trends in robotic surgery," *Int. J. Endurol.* **19**(8), 940–951 (2005).
2. J.-P. Merlet, *Parallel Robots* (Kluwer, Dordrecht, The Netherlands, 2000) pp. 31–54.
3. J.-P. Merlet, "Miniature In-Parallel Positioning System Mips for Minimally Invasive Surgery," *Proceedings of the World Congress on Medical Physics and Biomedical Engineering*, Nice, France (Sep. 14–19, 1997) pp. 141–147.
4. A. Darzi and S. Mackay, "Recent advances in minimal access surgery," *Int. Br. Med. J.* **324**(7328), 31–34 (2002).
5. T. Asao, H. Kuwano and E. Mochiki, "Laparoscopic surgery update for gastrointestinal malignancy," *Int. J. Gastroenterol.* **39**(4), 309–318 (2004).
6. G. S. Guthart and J. K. Salisbury, Jr., "The Intuitive™Telesurgery System: Overview and Application. *IEEE International Conference Robotics and Automation ICRA00*, vol. 1 (San Francisco, CA, Apr. 24–28, 2000) pp. 618–621.

7. F. Cepolina and R. C. Michelini, "Review of robotic fixtures for low-invasivenss surgery," *Int. J. Med. Robot. Comput. Assist. Surg.* **1**(1), 43–63 (2004).

8. M. J. H. Lum, D. Trimble, J. Rosen, K. Fodero, H. H. King, G. Sankaranarayanan, J. Dosher, R. Leuschke, B. Martin-Anderson, M. N. Sinanan and B. Hannaford, "Multidisciplinary Approach for Developing a New Minimally Invasive Surgical Robotic System," *IEEE/RAS-EMBS International Conference on Biomedical Robotics and Biomechatronics BioRob2006*, Pisa, Italy (Feb. 20–22, 2006).

9. J. Rosen and B. Hannaford, "Doc at a distance," *IEEE Spectr.* **43**(10), 34–39 (2006).

10. M. C. Çavuşoğlu, M. Cohn, F. Tendick and S. S. Sastry, "Laparoscopic telesurgical workstation," *Int. J. IEEE Trans. Robot. Autom.* **15**(4), 728–739 (1998).

11. J. Arata, M. Mitushi, W. Shin'ichi, K. Tanaka, T. Yoshizawa and M. Hashizume, "Development of a Dexterous Minimally-Invasive Surgical System with Augmented Force Feedback Capability," *IEEE/RSJ International Conference Intelligent Robots and Systems IROS2005*, Japan (Aug. 2–6, 2005) pp. 3207–3212.

12. T. Ortmaier, H. Weiss and V. Falk, "Design requirements for a new robot for minimally invasive surgery," *Int. J. Ind. Robot.* **31**(6), 493–498 (2004).

13. A. J. Madhani, G. Niemeyer and J. K. Salisbury, Jr., "The Black Falcon: A Teleoperated Surgical Instrument for Minimally Invasive Surgery," *IEEE/RSJ International Conference Intelligent Robots and Systems*, Victoria, Canada (Oct. 13–17, 1998) pp. 936–944.

14. J. Mamazza, C. M. Schlachta, P. A. Seshadri, M. O. Cadeddu and E. C. Poulin, "Needlescopic surgery," *Int. J. Surg. Endosc.* **15**(10), 1208–1212 (2001).

15. X. Kong and C. M. Gosselin, *Type Synthesis of Parallel Mechanisms*, Springer Tracts in Advanced Robotics, vol. **33** (2007).

16. M. Zoppi, D. Zlatanov and R. Molfino, "On the velocity analysis of interconnected chains mechanisms," *Int. J. Mech. Mach. Theory* **41**(11), 1346–1358 (2006).

17. M. Zoppi, W. Sieklicki and R. Molfino, "Design of a micro robotic wrist for needle laparoscopic surgery," *ASME J. Mech. Des.* **130**(10), 102306-1–102306-8 (2008).

18. J. K. Salisbury, Jr., "The heart of microsurgery," *ASME Mech. Eng. Mag.* **120**(12), 47–51 (1998).

19. H. Noma, T. Miyasato and F. Kishino, *A Palmtop Display for Dexterous Manipulation with Haptic Sensation* (ACM, New York, 1996) pp. 126–137.

20. A. Faraz and S. Payandeh, *Engineering Approaches to Mechanical and Robotic Design for Minimally Invasive Surgeries*, Springer International Series in Engineering and Computer Science (Kluwer Academic Publisher, 2000).

21. G. S. Ferzli and A. Fingerhut, "Trocar placement for laparoscopic abdominal procedures: A simple standardized method," *Int. J. Am. College Surg.* **198**(1), 163–173 (2004).

22. M. C. Cavusoglu, I. Villanueva and F. Tendick, "Workspace Analysis of Robotic Manipulators for a Teleoperated Suturing Task," *International Conference IEEE/RSJ:IROS*, Hawaii, (2001).

23. M. J. H. Lum, J. Rosen, B. Hannaford and M. N. Sinanan, "Optimization of a spherical mechanism for a minimally invasive surgical robot: Theoretical and exp. approaches," *Int. J. IEEE Trans. Biomed. Eng.* **53**(7), 1140–1145 (2006).

24. M. J. Fumo, A. K. Hemal and M. Menon, "Robotic Assisted Laparoscopic Radical Prostatectomy" **In** *Endourological Management of Urogenital Carcinoma* (S. Naito, Y. Hirao and T. Terachil, eds.) (Springer, Tokyo, 2006) pp. 175–190.

25. J. Luo, Z. Cai and Y. Huang, "Clinical experience of needle-laparoscopic cholecystectomy," *Int. J. Surg. Pract.* **4**(1), 17–19 (2000).

26. K. W. Lee, C. M. Poon, K. F. Leung, D. W. H. Lee and C. W. Ko, "Two-port needlescopic cholecystectomy: Prospective study of 100 cases," *Int. J. Hong Kong Med. J.* **11**, 30–35 (2005).

27. N. Tagaya, R. Kyu and K. Kubota, "Splenectomy using a completely needlescopic procedure: Report of three cases," *Int. J. Laparoendoscopic Adv. Surg. Techn.* **12**(3), 213–216 (2002).

28. J. D. Brown, J. Rosen, L. Chang, M. N. Sinanan and B. Hannaford, "Quantifying surgeon grasping mechanics in laparoscopy using the blue dragon system," *Studies in Health Technology and Informatics – Medicine Meets Virtual Reality*, Newport Beach, CA (January 2004).

29. M. Zoppi, D. Zlatanov and C. M. Gosselin, "Analytical kinematics models and special geometries of a class of 4-dof parallel mechanisms," *IEEE Trans. Robot.* **21**(6), 1046–1055 (2005).

30. M. A. Khan, M. Zoppi and R. Molfino, "4dof Parallel Architecture for Laparoscopic Surgery," **In** *Advances in Robot Kinematics ARK 2008* (J. Lenarcic, ed.) (Kluwer, Batz-sur-Mer, France, Jun. 22–26, 2008) pp. 119–126.

31. X. Zhang and C. A. Nelson, "Kinematic analysis and optimization of a novel robot for surgical tool manipulation." *ASME J. Med. Devices* **2** (2008).

32. D. A. McAffee and P. Fiorini, "Hand Controller Design Requirements and Performance Issues in Telerobotics," *International Conference on Advanced Robotics ICAR91*, vol. 1, Pisa, Italy (Jun. 19–22, 1991) pp. 186–192.

33. I. A. Bonev, D. Zlatanov and C. M. Gosselin, "Advantages of the Modified Euler Angles in the Design and Control of PKMs." **In** *Development Methods and Application Experience of Parallel Kinematics*. (R. Neugebauer, ed.) (Proceedings of the 3rd Chemnitz Parallel Kinematics Seminar PKS2002, vol. 16, Chemnitz, Germany, Apr. 23–25, 2002) pp. 429–440.

34. H. Z. Tan, X. D. Pang and N. I. Durlach, "Manual Resolution of Length, Force and Compliance," *International ASME 1992 Winter Annual Meeting*, vol. 42, Anaheim, CA (Nov. 1992) pp. 440. 13–18.